MOLECULAR ONCOLOGY 8 (2014) 1729–1746

available at www.sciencedirect.com

ScienceDirect

www.elsevier.com/locate/molonc

Senescent stroma promotes prostate cancer progression: The role of miR-210

Maria Letizia Taddei[a,*], *Lorenzo Cavallini*[a], *Giuseppina Comito*[a], *Elisa Giannoni*[a], *Marco Folini*[b], *Alberto Marini*[c], *Paolo Gandellini*[b], *Andrea Morandi*[a], *Gianfranco Pintus*[c], *Maria Rosaria Raspollini*[d], *Nadia Zaffaroni*[b], *Paola Chiarugi*[a,e]

[a]*Department of Experimental and Clinical Biomedical Sciences, University of Florence, Viale Morgagni 50, 50134 Florence, Italy*

[b]*Department of Experimental Oncology and Molecular Medicine, Fondazione IRCCS Istituto Nazionale dei Tumori, Via G. Amadeo 42, 20133 Milan, Italy*

[c]*Department of Biomedical Sciences, University of Sassari, Viale San Pietro 43/B 07100 Sassari, Italy*

[d]*Histology and Molecular Diagnostic, University Hospital Careggi, Viale G.B. Morgagni 85, 50134 Florence, Italy*

[e]*Center for Research, Transfer and High Education 'Study at Molecular and Clinical Level of Chronic, Inflammatory, Degenerative and Neoplastic Disorders for the Development on Novel Therapies', Italy*

ARTICLE INFO

Article history:
Received 15 January 2014
Received in revised form
10 July 2014
Accepted 11 July 2014
Available online 21 July 2014

Keywords:
Senescence
Prostate cancer
Tumor microenvironment
miR-210

ABSTRACT

We focused our interest on senescent human-derived fibroblasts in the progression of prostate cancer. Hypoxic senescent fibroblasts promote prostate cancer aggressiveness by inducing epithelial to mesenchymal transition (EMT) and by secreting energy-rich compounds to support cancer cell growth. Hypoxic senescent fibroblasts additionally increase: i) the recruitment of monocytes and their M2-macrophage polarization, ii) the recruitment of bone marrow-derived endothelial precursor cells, facilitating their vasculogenic ability and iii) capillary morphogenesis, proliferation and invasion of human mature endothelial cells. In addition, we highlight that overexpression of the hypoxia-induced *miR-210* in young fibroblasts increases their senescence-associated features and converts them into cancer associated fibroblast (CAF)-like cells, able to promote cancer cells EMT, to support angiogenesis and to recruit endothelial precursor cells and monocytes/macrophages.

Abbreviations: CAF, cancer associated fibroblast; CM, conditioned medium; COX, cyclooxygenase; EPC, endothelial progenitor cell; HIF, hypoxia-inducible factor; HPF, human prostate fibroblasts; HUVEC, human umbilical vein endothelial cells; IL, interleukin; EMT, epithelial mesenchymal transition; M-CSFR, macrophage-colony stimulating factor receptor; MMPs, matrix metallo proteinases; RS, replicative senescence; ROS, reactive oxygen species; SA-β-Gal, senescence-associated β-Galactosidase; SASP, senescence-associated secretory phenotype; SDF-1, stromal cell-derived factor 1; SIS, stress-induced senescence; VEGF, vascular endothelial growth factor.

* *Corresponding author*. Dipartimento di Scienze Biomediche Sperimentali e Cliniche, Viale Morgagni 50, 50134 Firenze, Italy. Tel.: +39 055 2751236; fax: +39 055 7830303.

E-mail address: marialetizia.taddei@unifi.it (M.L. Taddei).

http://dx.doi.org/10.1016/j.molonc.2014.07.009

1. Introduction

It is established that tumor incidence is strongly associated with age in mammalian species. Although somatic mutations that accumulate in epithelial cells during aging are the major determinants of tumor development (DePinho, 2000; Dolle et al., 2002), it has been recently reported that a permissive microenvironment has a key role in tumorigenesis (Hanahan and Weinberg, 2011; Pietras and Ostman, 2010). In this scenario, stromal senescent cells could alter the microenvironment and contribute to increase the risk of carcinoma with advancing age (Krtolica et al., 2001). Cell senescence is characterized by an irreversible loss of proliferative ability of normal human cells in culture (Hayflick, 1965). This can be caused by the progressive telomere shortening or by a variety of stimuli like DNA damage, oncogenes expression or chromatin modification and epigenetic reprogramming (Aisner et al., 2002; Chen et al., 1995; Di et al., 1994; Kim Sh et al., 2002; Krtolica and Campisi, 2002; Ogryzko et al., 1996; Robles and Adami, 1998; Serrano et al., 1997). Despite the growth arrest, senescent cells remain metabolically active, exhibit a classical morphology and secrete several soluble or insoluble factors, the so called senescence-associated secretory phenotype (SASP), which can disrupt the function and the structure of the surrounding tissue and promote carcinogenesis and tumor progression (Coppe et al., 2010; Krtolica and Campisi, 2002). Indeed, SASP has been implicated in a wide variety of age-related pathologies like cardiovascular diseases, osteoporosis and neurodegenerative diseases as well as in promoting tumor development and progression (Campisi et al., 2011; Tchkonia et al., 2013). Furthermore, senescent human fibroblasts can disrupt the morphological and functional differentiation of pre-malignant mammary epithelial cells and induce malignant transformation (Parrinello et al., 2005). Moreover, senescent stromal cells are able to transform immortalized, non-neoplastic breast epithelial cells and promote progression of neoplastic cell lines (Krtolica et al., 2001). In addition, Bavik et al. demonstrated that senescent prostate fibroblasts stimulate the growth of pre-neoplastic and neoplastic prostate epithelium through the secretion of paracrine factors able to influence the adjacent prostate epithelial growth (Bavik et al., 2006). In keeping with these data, *in vivo* studies demonstrated that regions adjacent to cancer epithelium are enriched in senescent stromal cells (Yang et al., 2006).

Recently, a panel of microRNAs (miRNAs) have been identified to be differentially regulated in senescent human lung fibroblasts (WI-38) compared to the matched pre-senescent fibroblasts. Crucially, *miR-210* results up regulated in senescent fibroblasts and its overexpression induces DNA damage, reduces cell proliferation and increases oxidative stress (Faraonio et al., 2012).

In this study we investigated the role of senescent stroma in the onset and progression of prostate cancer (PCa) highlighting the central role of hypoxic senescent stroma in sustaining the development of a pro-tumorigenic microenvironment by recruiting/organizing vessels and supporting inflammation. In particular, we demonstrated that *miR-210* overexpression increased senescence-associated features (e.g. SASP and DNA-damage foci) in young fibroblasts and converted them into CAF-like cells. These senescent fibroblasts can induce EMT in PCa cells, support tumor angiogenesis and recruit endothelial precursor cells, thus contributing to cancer progression.

2. Material and methods

2.1. Materials

Unless otherwise specified all reagents were obtained from Sigma. Anti E-cadherin, anti vimentin, anti Glut-1, anti MCT4, anti MCSF-R, anti actin, anti COX-2, anti-$p16^{INK4}$ antibodies were from Santa Cruz; anti Collagen1, anti α-sma, anti IL-6, anti IL8, anti-$p21^{WAF1}$ antibodies were from AbCam, anti human phospho-histone H2AX (S139) antibodies and the Matrigel were from R&D System; anti-vinculin antibody was from Sigma Aldrich. Anti CD163 antibodies were from Epitomics and anti CD68 antibodies were from Dako. Anti Nitric oxide synthase (inducible) antibodies was from Enzo Life Sciences. Anti mouse Alexa 488 antibody was from Molecular Probes. ELISA Kits (IL-10 and IL-12) were from Invitrogen. Co-cultures separation was performed by MACS MicroBeads and MACS Column Technology patented by Miltenyi Biotec.

2.2. Cell cultures

Human prostate cancer cells (PC3) and human umbilical vein endothelial cells (HUVECs) were purchased from the European Collection of Cell Cultures (ECACC). PC3 cells were cultured in DMEM containing 10% FBS, while endothelial cells were cultured on gelatin 1% coated dishes in EGM-2 medium (Lonza). Endothelial progenitor cells (EPCs) were isolated from human umbilical cord blood as previously described (Margheri et al., 2011). Human prostate fibroblasts (HPFs) were isolated from surgical explants of patients affected by benign prostatic hyperplasia (Giannoni et al., 2010).

To induce stress-activated senescence cells were treated for 2 h at 37 °C with 500 μM hydrogen peroxide. After treatment, cells were left to recover for 1 week. For replicative senescence, fibroblasts were cultured for 35 doublings. Replicative exhaustion was confirmed in senescent cells which showed <5% BrdU incorporation and >70% SA-β-Gal staining, while pre-senescent fibroblasts showed >75% BrdU incorporation and <15% SA-β-Gal staining.

2.3. β-Galactosidase staining

Cells were fixed for 5 min at room temperature with 3% paraformaldehyde in PBS. After two washes in PBS cells were incubated for 24 h at 37 °C in freshly prepared senescence-associated β-Galactosidase (SA-β-Gal) staining solution containing 1 mg/ml 5-bromo-4-chloro-3-indolyl β-D-galactopyranoside (X-Gal), 5 mM potassium ferrocyanide, 5 mM potassium ferricyanide, 150 mM NaCl, 2 mM $MgCl_2$ and 40 mM citric acid, pH6.0. SA-β-Gal staining is microscopically revealed by the presence of a blue, insoluble precipitate within the cell.

2.4. Co-cultures separation

PC3 and fibroblasts were plated in a 1:3 ratio. After 24 h cells were serum starved and incubated for additional 24 h in hypoxic condition (1% O_2). Cells were then detached with Accutase (Life Technologies) and incubated for 30 min with Anti-fibroblast MicroBeads (Miltenyi Biotec cat 130-050-601) to selectively magnetically label fibroblasts within the co-culture. The cell suspension is then loaded onto a MACS Column (Miltenyi Biotec cat 130-042-201) which is placed in the magnetic field of a MACS Separator (Miltenyi Biotec cat 130-042-102) to retain the magnetically labeled fibroblasts within the column while unlabeled PC3 run through.

2.5. Preparation of conditioned media

Conditioned media (CM) were obtained from pre-senescent or senescent fibroblasts grown to sub-confluence, then serum starved for 24 h and cultured for additional 24 h in hypoxic condition (1% O_2). CM were then harvested, clarified by centrifugation, and used freshly.

2.6. Telomere length analysis

Total genomic DNA was extracted from pre-senescent and senescent fibroblasts by DNAzol® (Life Technologies, Monza, Italy), according to the manufacturer's instructions. Five micrograms of DNA were digested with Hinf I (10 U/μl, New England Biolabs, Ipswich, MA) and resolved on a 1.2% agarose gel by pulsed field gel electrophoresis (5 V/cm, 0.5–5 s switch times, 14 °C for 17 h). Lambda DNA-Hind III digest (Bio-Rad Laboratories, Segrate, Italy) was used for size determination of telomere restriction fragments (TRF). After UV cross-linking (60 mJ/cm^2 for 1 min), denaturation (1.5 M NaCl; 0.5 M NaOH) and neutralization (3 M NaCl; 0.5 M Tris pH 7.5), DNA was transferred onto nylon membranes (Hybond N, GE Healthcare Europe GmbH, Milano, Italy). Filters were then hybridized for 3 h at 42 °C in rapid hybridization buffer (Roche Applied Science, Monza, Italy) in the presence of digoxigenin-labeled telomeric probe $(TTAGGG)_4$. TRFs were detected by autoradiography using the DIG Luminescent Detection Kit (Roche Applied Science), according to the manufacturer's instructions. Autoradiographs were scanned (ImageScanner III, GE Healthcare) and densitometric analysis was carried out on gray scale images using ImageJ 1.46r. Mean telomere length was calculated as TL = $\sum$ (ODi)/$\sum$ (ODi/MWi) where ODi and MWi are the optical density and the molecular weight at position i, respectively (Kimura et al., 2010). The upper and lower limits of TRF distribution for calculation of mean TRF length were set at 20 and 2 kb, respectively.

2.7. Western blot analysis

Fibroblasts, PC3 cells or macrophages derived from our experimental conditions were lysed for 20 min on ice in 500 μl of RIPA lysis buffer (50 mM Tris–HCl, pH 7.5, 150 mM NaCl, 1% Triton X-100, 2 mM EGTA, 1 mM sodium orthovanadate, 1 mM phenylmethanesulphonyl-fluoride, 10 mg/ml aprotinin, 10 mg/ml leupeptin). Twenty micrograms of total proteins were loaded on SDS–PAGE, separated and transferred onto nitrocellulose. The immunoblots were incubated in 3% bovine serum albumin, 10 mmol/L Tris–HCl (pH 7.5), 1 mmol/L EDTA, and 0.1% Tween 20 for 1 h at room temperature, probed first with specific antibodies and then with appropriate secondary antibodies. Bound antibodies were detected using the Novex ECL, HRP Chemiluminescent substrate Reagent Kit (Life Technologies). Filters were autoradiographed and images were acquired by Biospectrum Imaging System (Ultra-Violet Products Ltd, Cambridge, UK).

2.8. Invasion assay

After co-culture separation, 8×10^4 PC3 cells were seeded onto Matrigel-precoated Boyden chamber (8 mm pore size, 6.5 mm diameter, 12.5 μg Matrigel/filter). In the lower chamber, complete medium was added as chemoattractant. Following 24 h of incubation, the inserts were removed and the non-invading cells on the upper surface were removed with a cotton swab. The filters were then stained using the Diff-Quik kit (BD Biosciences) and photographs of randomly chosen fields are taken. For monocytes recruitment 10^5 cells were seeded onto 5 μm-pore-size polyvinylpyrrolidone-free polycarbonate filters. Migration towards conditioned media from pre-senescent or senescent cells was allowed for 2 h at 37 °C. For HUVEC invasion and EPC migration, 5×10^4 cells were seeded onto Boyden chamber with or without Matrigel (8 mm pore size, 6.5 mm diameter, 12.5 μg Matrigel/filter).

2.9. Proliferation assay

2×10^3 HUVEC cells were seeded in 96-multiwell plates and serum starved for 24 h before the addition of conditioned media for 48 h. Cell growth was stopped by removing the medium and by the adding a 0.5% crystal violet solution in 20% methanol. After 5 min of staining, fixed cells were washed with PBS and solubilized with 200 μl/well of 0.1 M sodium citrate, pH 4.2. The absorbance at 595 nm was evaluated using a microplate reader.

2.10. Real time RT-PCR

Total RNA from fibroblasts or PC3 cells was extracted using RNeasy (Qiagen) according to the manufacturer's instructions. Strands of cDNA were synthesized using a high capacity cDNA reverse transcription kit (Applied Biosystem) using 1 μg of total RNA. For quantification of mRNA expression, Real-Time PCR, using Power SYBR green dye (Applied Biosystem) was done on a 7500 Fast Real Time PCR system (Applied Biosystem). The primers were IL-6: 5′-TCAAACTGCATAGC CACTTTCC-3′ (forward), 5′-AGTTCCTGCAGTCCAGCCTGAG-3′ (reverse); IL-8: 5′-CTGGCCGTGGCTCTCTTG-3′ (forward), 5′-TTAGCACTCCTTGGCAAAACTG-3′ (reverse); VEGF-A 5′-TACC TCCACCATGCCAAGTG-3′ (forward), 5′-ATGATTCTGCCCTCC TCCTTC-3′ (reverse); MMP3: 5′-TTCCTGGCATCCCGAAGTGG-3′ (forward), 5′-ACAGCCTGGAGAATGTGAGTGG-3′ (reverse). Data were normalized to those obtained with Glyceraldehyde-3-phosphate dehydrogenase primers. Results (mean ± SD) are the mean of three different experiments.

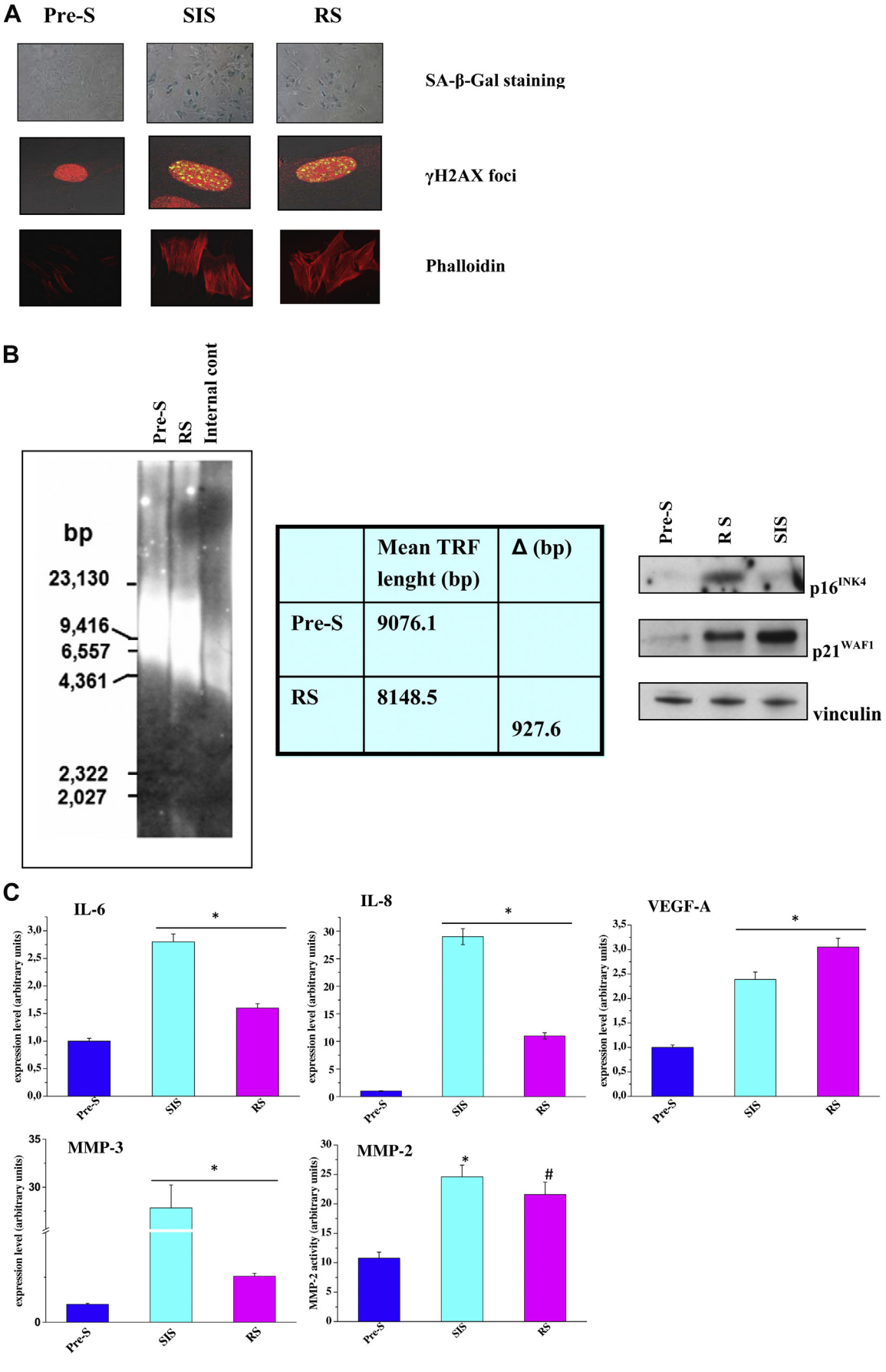
A
Pre-S
SIS
RS
SA-β-Gal staining
γH2AX foci
Phalloidin
B
Pre-S
RS
Internal cont
bp
23,130
9,416
6,557
4,361
2,322
2,027
Mean TRF lenght (bp)
Δ (bp)
Pre-S
9076.1
RS
8148.5
927.6
Pre-S
R S
SIS
p16INK4
p21WAF1
vinculin
C
IL-6
IL-8
VEGF-A
MMP-3
MMP-2
expression level (arbitrary units)
MMP-2 activity (arbitrary units)
Pre-S
SIS
RS
*
#

For what concerns *miRNA* expression analysis, total RNA, including small RNAs, was purified using RNeasy kit from Qiagen. The reverse transcription reaction of 1 μg of total RNA was carried on using miScript II RT kit (Qiagen) and the quantification of *miR210* expression level was assessed by Real Time PCR using miScript SYBR Green PCR kit and miScript Primer Assay-HsmiR-210 from Qiagen. SNORD61 was used as normalizer (miScript Primer Assay-HsSNORD61 from Qiagen).

2.11. Macrophages differentiation

Human monocytes were obtained from normal donor buffy coat by gradient centrifugation using Ficoll (Histopaque-1077). Non-adherent cells were removed and purified monocytes were incubated for 7 days in RPMI 1640 supplemented with 10% FBS and 50 ng/ml macrophage-colony stimulating factor (M-CSF) to obtain macrophages. M1 macrophages were polarized by stimulating overnight with Lipopolysaccharide (100 ng/ml) (Peprotech) and IFNγ (100 ng/ml) (Peprotech). M2 macrophages were polarized by stimulating over-night with interleukin-4 (IL-4) (20 ng/ml) (Peprotech). M2-like macrophages were obtain by culturing monocytes for 7 days in RPMI 1640 10% FBS plus 50% of conditioned medium from pre-senescence or senescent cells.

2.12. Matrigel angiogenesis in vitro

Fifty microliters of Matrigel 1 mg/ml was added to each well of a 96-well plate and then placed in a humidified incubator at 37 °C for 30 min. HUVECs (2×10^4 cells/well) were added to the Matrigel-coated plates in the presence of 200 μl conditioned media of senescent or pre-senescent cells. The effects on the morphogenesis of endothelial cells were recorded after 6 h with an inverted microscope equipped with CCD optics and a digital analysis system. Results were quantified by measuring the joint numbers in the field.

2.13. Transfection

miR-210 precursor (Pre-miR™) and negative controls (*mir*Vana™ miRNA Mimic, Negative Control #1 and Pre-miR™ miRNA Precursor Negative Control #1) were purchased from Life Technologies, miRCURY LNA Inhibitor was from Exiqon. Fibroblasts were transfected for 4 h at 37 °C with 20 nmol/L miRNA precursors or miRCURY LNA Inhibitor using Lipofectamine-2000 (Life Technologies), according to the manufacturer's instructions. miR-210 mRNA expression was assessed by qRT-PCR using miScript SYBR Green PCR Kit.

2.14. Lactate assay

Lactate was measured in the cultured media with Lactate Assay kit (Source Bioscience Life Sciences) according to the manufacturer's instructions. Results were normalized for total cellular protein.

2.15. Lactate dehydrogenase activity assay

Cell lysis was performed at 4 °C in 50 mM Tris, pH 7.4, containing 5 mM dithiothreitol and Sigma protease inhibitors mix (1/100, v/v). After 30 min of incubation on ice, lysates were sonicated and centrifuged at 12,000 *g* in a microcentrifuge at 4 °C for 30 min. Supernatants were quantified with respect to protein content by Bradford method. Lactate dehydrogenase (LDH) activity was assayed at 37 °C continuously following the decrease of NADH absorbance at 340 nm. Twenty microliters of supernatants were used to performed the analysis in 1 mL of reaction mix as follows: 500 μL TRAP/3 (Triethanolamine 100 mM, EDTA 10 mM, pH 7.6), 440 μL deionized H_2O, 20 μL NADH 10 mM, 20 μL sodium pyruvate 40 mM.

2.16. Ketone bodies production

Cells were maintained in DMEM without phenol-red and media are then collected. Keto-acid concentration was measured according to the manufacturer's instructions using the β-Hydroxy-butyrate Assay kit (BioVision). Results were normalized for total protein amounts.

2.17. Immunocytochemistry

After washing with PBS, cells were fixed with 3.7% formaldehyde solution in PBS for 20 min at 4 °C. Then, after extensive washes in PBS, cells were permeabilized with 0.1% Triton X-100 in PBS and then stained with a 50 μg/ml fluorescent phalloidin conjugate solution in PBS, phalloidin-TRITC, for 1 h at room temperature or with anti-human phospho histone H2AX (S139) antibodies and then with Anti mouse Alexa 488 antibodies. After several washes with PBS, the coverslides

Figure 1 – Human prostate fibroblasts induced to senesce by oxidative stress or cellular replication exhibit a senescence-associated secretory phenotype. A) Representative images of pre-senescent fibroblasts, replicative exhausted fibroblasts, or fibroblasts treated with 500 μM H_2O_2 for 2 h at 37 °C stained for SA-β-Gal, or fixed and examined by immunofluorescence for H2AX phosphorylated on Ser139 (γ-H2AX) and counterstained with propidium iodide or Phalloidin. B) Representative southern blot image (left) showing the distribution of telomere restriction fragments in pre-senescent and replicative exhausted fibroblasts. Internal control: restriction-digested DNA from the telomerase-positive human HeLa cells; numbers on the left indicate the molecular size marker (bp: base pairs). Table shows mean telomere length in each sample, calculated as reported in the Material and Methods section, and the difference between mean values (Δ) observed in RS compared to pre-senescent fibroblasts. Representative western immunoblotting (right) showing the expression levels of the cyclin-dependent kinase inhibitors $p16^{INK4}$ and $p21^{WAF1}$ in pre-senescent, replicative exhausted and H_2O_2-treated fibroblasts. An anti-vinculin antibody was used to ensure equal protein loading. C) Monolayers of cells treated as in A) were serum starved for 24 h and then incubated for additional 24 h in hypoxic condition (i.e., 1% O_2). Total RNA was extracted and IL-6, IL-8, VEGF-A, MMP-3 mRNA expression level were analyzed by qRT-PCR. MMP-2 activity was assayed by gelatine zymography and a representative bar graph is shown. Results are representative of three experiments with similar results. *$p < 0.005$ senescent cells *vs* pre-senescent cells. #$p < 0.001$ senescent cells *vs* pre-senescent cells.

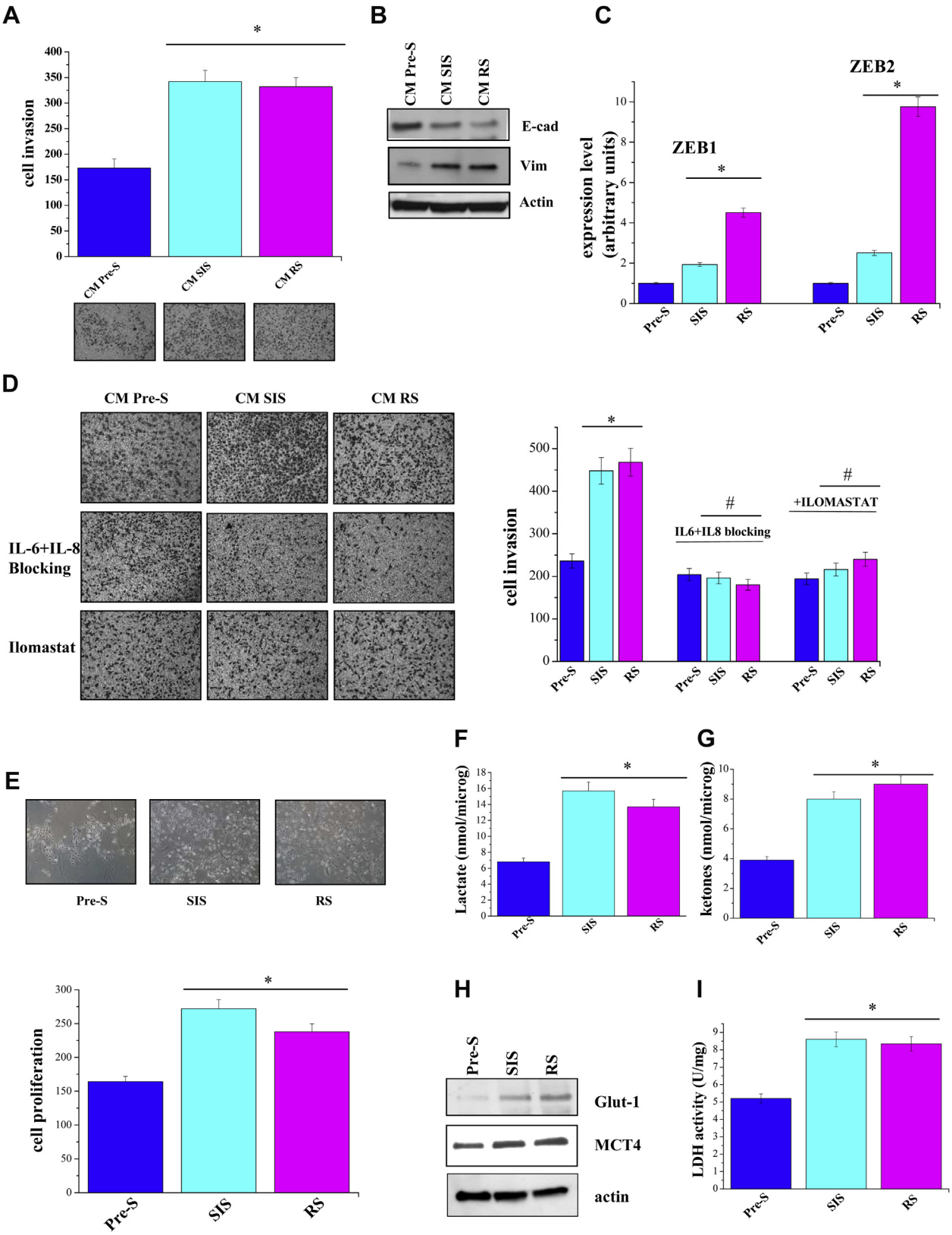

Figure 2 – Senescent fibroblasts induce both a pro-invasive phenotype and a trophic effect on PCa cells. A) Co-cultures of fibroblasts and PC3 were serum starved for 24 h and incubated for additional 24 h in hypoxic condition (1% O_2). Cells were then separated and 8 × 10^4 PC3 cells were allowed to invade in a Boyden Chamber. Invading cells were counted, and a bar graph, representative of six randomly chosen fields, is shown. *$p < 0.005$ senescent cells *vs* pre-senescent cells. B) PC3 cells were treated as in A), cell lysates were obtained to evaluate E-cadherin and vimentin amounts. C) PC3 cells were treated as in A), total RNA was extracted and ZEB1 and ZEB2 mRNA expression level was quantified by qRT-PCR. The results are representative of three experiments with similar results. *$p < 0.005$ senescent cells *vs* pre-senescent cells. D) 8 × 10^4 PC3 cells,

were mounted with glycerol plastine and then observed under a confocal fluorescence microscope (Leica).

2.18. Gene expression analysis of publicly available datasets

Data were obtained mapping miR210HG (44211_at), MMP3 (437_at) and IL8 (35372_r_at) to GSE6919 datasets; IL6 (ID564) to GSE21032 and MMP2 (39007_at) to Welsh dataset (Welsh et al., 2001). Data were retrieved from GEO profiles or Oncomine (www.oncomine.org), normalized and log2 scaled (if needed), median centered and statistical analysis was performed using Prism software (GraphPad Software, La Jolla, CA, USA). Data were compared using Student's *t*-test or one-way ANOVA as indicated in Figure legend.

2.19. Statistical analysis

Data are presented as means ± SD from at least three independent experiments. Statistical analysis of the data was performed by Student's *t* test. *p* values of ≤ 0.05 were considered statistically significant.

3. Results

3.1. Senescent fibroblasts induce a pro-invasive and proliferative phenotype of PCa cells

Cell senescence was first described as the process that limits the proliferation of normal cells in culture (Hayflick, 1965). This event is mainly due to the progressive telomere shortening during cell replication, but can also occur following oxidative stress, expression of distinct oncogenes and epigenetic perturbations in chromatin organization (Aisner et al., 2002; Chen et al., 1995; Di et al., 1994; Kim Sh et al., 2002; Krtolica and Campisi, 2002; Ogryzko et al., 1996; Robles and Adami, 1998; Serrano et al., 1997). In this study, we used primary prostate fibroblasts induced to senesce by replication in culture (RS) or by treatment with H_2O_2 (SIS) in comparison to pre-senescent cultures. As shown in Figure 1A, both experimental conditions are able to induce senescence as demonstrated by the increase in SA-β-Galactosidase activity (SA-β-Gal) and the accumulation of senescence-associated γH2AX foci in cell nuclei. In addition, senescent cells exhibit a classical morphology characterized by increased granularity, enlarged and flattened shape as evidenced by anti-phalloidin staining. Moreover, cells undergoing RS were characterized by shortened telomeres (mean telomere length: 8.1 kb) compared to non-senescent fibroblasts (mean telomere length: 9.1 kb) (Figure 1B). Consistently, a marked accumulation of the cyclin-dependent kinase inhibitors $p16^{INK4}$ and $p21^{WAF1}$ occurred in RS compared to pre-senescent cells and a pronounced accumulation of $p21^{WAF1}$ was also observed in SIS fibroblasts, dealing with the induction of premature senescence (Figure 1B). Furthermore, both experimental conditions lead to the activation of SASP, as monitored by secretion of several inflammatory and angiogenic cytokines, such as IL-6, IL-8, VEGF-A, MMP3, MMP2 (Figure 1C). We performed these experiments in 1% O_2, since senescent fibroblasts secrete higher levels of many SASP-related factors in hypoxic condition rather than in 20% O_2 (Coppe et al., 2008). Additionally, the hypoxic experimental setting is very close to the actual environment in which tumor cells grow and progress towards malignancy (Harris, 2002). We next investigated whether senescent fibroblasts co-cultured with prostate cancer cells are able to affect the behavior of the neighboring cancer cells. As shown in Figure 2A–C hypoxic senescent cells promote an increase of three-dimensional matrix invasiveness of PCa cells. Indeed, hypoxic senescent fibroblasts elicit a clear EMT in PC-3 cells as demonstrated by the expression of known EMT markers. Specifically we observed the up-regulation of ZEB1, ZEB2 and vimentin and the down-regulation of E-cadherin (Figure 2B,C). As shown in Figure 2D, blocking IL-6, IL-8 or MMPs by specific antibodies or Ilomastat, respectively, partially reverts the increased invasiveness of PC3 cells, suggesting that SASP is the driving force to direct a pro-invasive effect in PC3 cells stimulated by hypoxic senescent cells. Besides, the contact with senescent cells exerts a trophic effect on PCa cells as shown by the increase of PC3 cell proliferation when co-cultured with senescent cells (Figure 2E). These data are in line with our previous findings of a reciprocal interplay between CAFs and prostate cancer cells. This bidirectional interaction has been shown to be importantly mediated by a hypoxia-inducible factor 1 (HIF-1) dependent mechanism in which increased stromal production of lactate sustains cancer cell growth (Fiaschi et al., 2012). Similarly, hypoxic senescent fibroblasts increased the glucose importer Glut-1 and the lactate exporter MCT4. Accordingly, they secrete energy-rich metabolites, such as L-lactate and ketone bodies that support tumor cell growth

after 24 h of serum starvation were seeded into the upper compartment of Boyden chamber. Cells were allowed to migrate through the filter coated with Matrigel toward the lower compartment filled with CM from pre-senescent or senescent fibroblasts in the presence of 0.8 μg/ml IL-6 and 1 μg/ml IL-8 blocking antibodies or 50 μM Ilomastat. Cell invasion was evaluated after Diff-Quick staining by counting cells in six randomly chosen fields. The bar graphs represent the number of invading cells in six randomly chosen fields of triplicate experiments. *$p < 0.005$ senescent cells *vs* pre-senescent cells; #$p < 0.005$ treated senescent cells *vs* untreated senescent cells. E) 5×10^4 PC3 were plated with fibroblasts in a ratio 1:3 for 48 h. The co-culture were serum starved for 24 h and incubated for additional 24 h in hypoxic condition (1% O_2). Cells were then separated and PC3 cells were counted to evaluated cell growth. Proliferation index has been reported in the bar graph. *$p < 0.005$ senescent cells *vs* pre-senescent cells. F–G) Pre-senescent or senescent fibroblasts were serum starved for 24 h and incubated for additional 24 h in hypoxic condition (1% O_2), conditioned media are then collected and lactate assay and ketone bodies assay were performed. The results are representative of three experiments with similar results. *$p < 0.005$ senescent cells *vs* pre-senescent cells. H) Cell treated as in A) were lysed and subjected to Glut-1, MCT4 and actin immunoblot analysis or a Lactate dehydrogenase activity assay performed (I). The results are representative of three experiments with similar results. *$p < 0.005$ senescent cells *vs* pre-senescent cells.

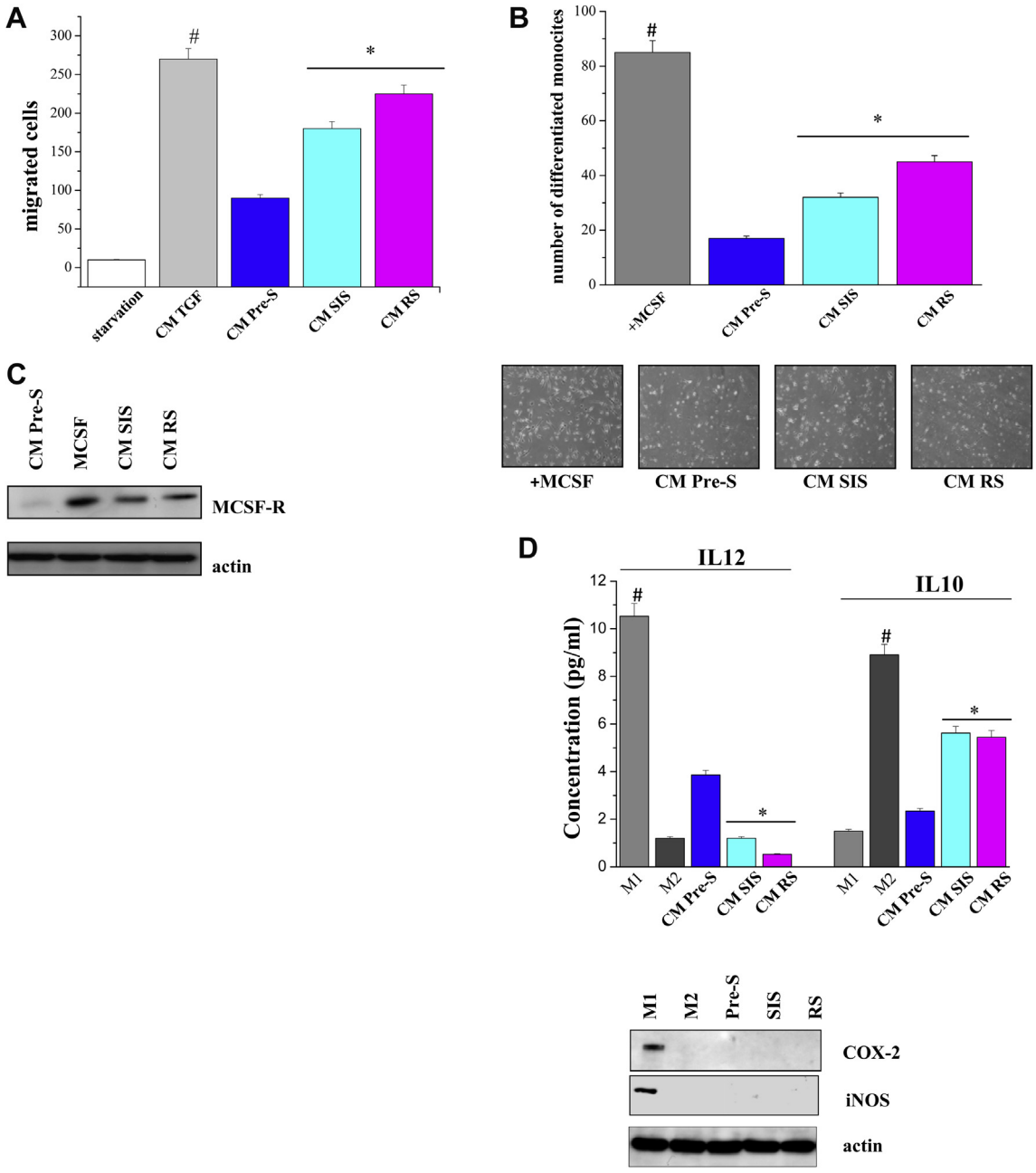

Figure 3 – Conditioned media from senescent fibroblasts recruit human monocytes and differentiate them into M2 macrophages. A) Monocytes isolated from normal donor buffy coat were serum starved and then were allowed to migrate for 2 h toward CM of pre-senescent or senescent fibroblasts. As positive control CM of fibroblasts activated with 10 ng/ml TGF-β for 24 h was used. #$p < 0.005$ TGF-β-treated cells *vs* starvation; *$p < 0.005$ CM senescent cells *vs* CM pre-senescent cells. B) Human monocytes were cultured for 7 days in CM from pre-senescent or senescent fibroblasts. As a positive control of differentiation, monocytes were cultured for 7 days with MCSF (50 ng/ml). Differentiated macrophages were counted, and a bar graph, representative of six randomly chosen fields, is shown. #$p < 0.005$ MCSF treated cells *vs* untreated; *$p < 0.005$ CM senescent cells *vs* CM pre-senescent cells. C) Monocytes were cultured as in B). Cells were lysed and the expression of MCSF-R and actin was evaluated by immunoblots. D) M1 and M2 macrophages were obtained as reported in the Material and Methods section. Cells were treated as in B and the levels of IL-12 or IL-10 were measured by ELISA test. #$p < 0.005$ CM M1 cells *vs* CM M2 or CM fibroblasts; *$p < 0.005$ CM senescent cells *vs* CM pre-senescent cells. Cell lysates were subject to immunoblot analysis to evaluate the expression of COX-2, iNOS and actin.

(Figure 2F–H). In addition, also Lactate dehydrogenase (LDH) activity is increased in senescent fibroblasts (Figure 2I). Thus, hypoxic senescent fibroblasts have both a promoting effect on tumor invasiveness and a trophic effect by interfering with the metabolism of cancer cells.

3.2. *Senescent fibroblasts promote macrophage differentiation and angiogenesis*

We have previously demonstrated that CAFs promote the recruitment of monocytes and macrophage differentiation

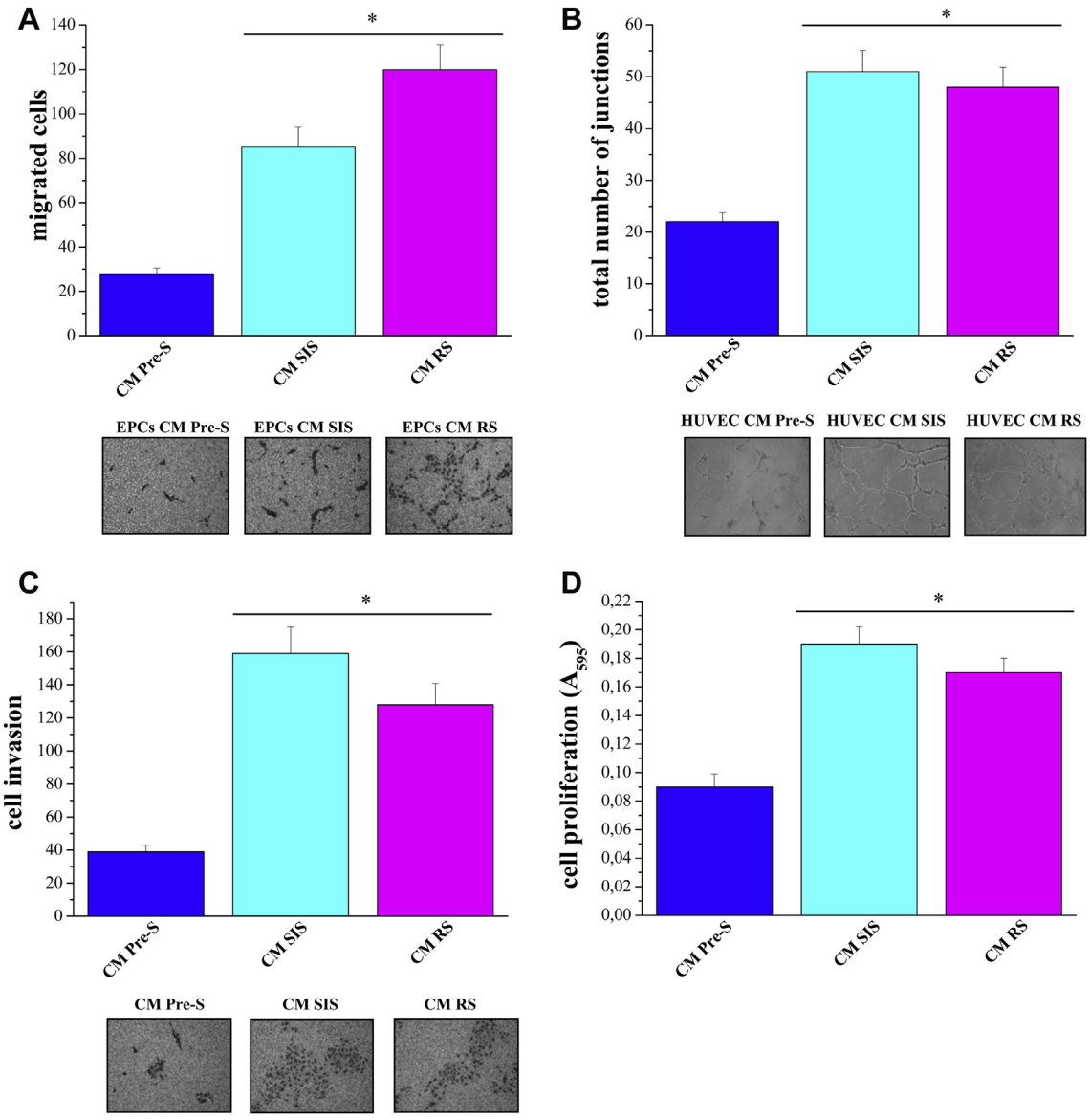

Figure 4 – Conditioned media from senescent fibroblasts increase *in vitro* angiogenesis. A) EPC cells, after 24 h of serum starvation, were seeded into the upper compartment of a Boyden chamber. Cells were allowed to migrate through the filter toward the lower compartment containing CM of pre-senescent or senescent fibroblasts medium. Cell migration was evaluated after Diff-Quick staining by counting cells in six randomly chosen fields. The results are representative of three experiments with similar results. *$p < 0.005$ CM senescent cells *vs* CM pre-senescent cells. B) HUVECs were seeded on Matrigel coated multiwell in the presence of CM of pre-senescent or senescent cells for 6 h at 37 °C. Cord formation was examined by phase-contrast microscopy. The total number of junctions for optical field is counted. Results are representative of three independent experiments. *$p < 0.005$ CM senescent cells *vs* CM pre-senescent cells. C) HUVEC cells, after 24 h of starvation in 1% serum were seeded into the upper compartment of Boyden chamber. Cells were allowed to migrate through the Matrigel-coated filter toward the lower compartment filled with CM of pre-senescent or senescent fibroblasts. Cell invasion was evaluated after Diff-Quick staining by counting cells in six randomly chosen fields. The results are representative of five experiments with similar results. *$p < 0.005$ CM senescent cells *vs* CM pre-senescent cells. D) 2×10^3 HUVECs were seeded in triplicate in 96-multiwell plates and serum starved for 24 h. Cells were grown for 48 h at 37 °C in the presence of CM of pre-senescent or senescent fibroblasts. Cell proliferation was evaluated after Crystal Violet staining. The results are representative of three experiments with similar results. *$p < 0.005$ CM senescent cells *vs* CM pre-senescent cells.

towards a pro-tumorigenic M2 phenotype (Comito et al., 2014). Here, we investigated whether senescent fibroblasts are able to recruit monocytes and eventually to differentiate them into macrophages. We observed that CM from hypoxic senescent stroma efficiently recruits circulating monocytes (Figure 3A). In addition, incubation of human blood monocytes with CM from hypoxic senescent fibroblasts promotes their differentiation to macrophages as demonstrated by morphological changes (Figure 3B) and by M-CSF receptor (M-CSFR) expression level increase (Figure 3C). Moreover, the absence of cyclooxygenase-2 (COX-2) and iNOS, as well as IL-10 and IL-12 production, demonstrated that macrophage

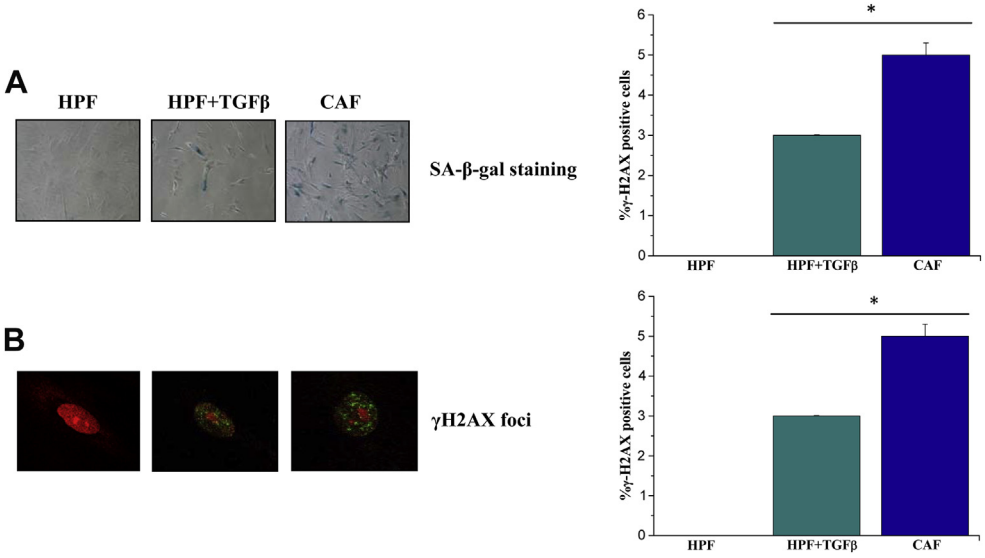

Figure 5 – Activated fibroblasts are SA-β-Gal and γ-foci positive. A) HPFs, CAFs or *in vitro* activated CAFs were stained for SA-β-Gal. Counts of at least 200 cells were averaged and expressed as percent of positive SA-β-Gal staining ±SD. *$p < 0.005$ HPF + TGFβ or CAF *vs* HPF. B) Cell treated as in A) were fixed and examined by immunofluorescence for H2AX phosphorylated on Ser139 (γ-H2AX) and counterstained with propidium iodide. Counts of at least 200 cells were averaged and expressed as percent of γ-foci positive staining ±SD. *$p < 0.005$ HPF + TGFβ or CAF *vs* HPF.

differentiation is polarized towards the M2 phenotype. Indeed we observed undetectable level of COX-2 and iNOS and an IL-12^{low} and IL-10^{high} production (Figure 3D). Thus, CM from hypoxic senescent stroma causes macrophage polarization towards the pro-tumorigenic M2 phenotype, contributing to an immunosuppressive microenvironment.

We next investigated the role of hypoxic senescent stroma on tumor vascularization and neo-angiogenesis, other key phenomena in cancer growth and metastasis. First, we assessed the ability of senescent cells to recruit endothelial progenitor cells (EPCs) isolated from human umbilical cords in a chemoattraction assay. CM of senescent fibroblasts cultured in low-oxygen condition, positively influence the recruitment of EPCs suggesting a direct involvement of such compartment in tumor vascularization (Figure 4A). To better investigate the neo-angiogenesis process, we performed an *in vitro* capillary morphogenesis assay: HUVEC cells were exposed to CM from hypoxic senescent or pre-senescent fibroblasts in Matrigel-coated plates. As shown in Figure 4B, CM from hypoxic senescent stroma produced a marked increase in capillary-like network formation already appreciable after 6 h of treatment. As shown in Supplementary Figure 1, blocking of IL-6, IL-8 with selective antibodies or MMPs with MMPs inhibitor Ilomastat decrease cell capillary morphogenesis, suggesting that SASP is involved in the neo-angiogenesis process. In agreement with a central role of senescent stroma in angiogenesis, CM derived from senescent fibroblasts were also able to stimulate both invasion and proliferation of HUVEC as monitored by invasion and proliferation assays (Figure 4C,D). These results strongly support the concept that SASP is crucial to develop a capillary network that facilitates tumor oxygenation and therefore cancer growth.

3.3. *Role of* miR-210 *in the functional correlation between fibroblast activation and senescence*

We have observed that many distinctive features of cell senescence resemble those of fibroblasts activation. Indeed, both CAFs and senescent fibroblasts can induce EMT of cancer cells, increase their trophism and interfere with the behavior of microenvironmental neighboring components like monocytes and endothelial cells (Comito et al., 2014; Fiaschi et al., 2012; Giannoni et al., 2011). Furthermore, many cytokines typical of SASP are pro-inflammatory cytokines that could also be secreted by activated fibroblasts (Bavik et al., 2006; Cirri and Chiarugi, 2012; Coppe et al., 2008; Giannoni et al., 2010). Firstly, we investigated whether *in vitro* activated HPFs or CAFs share some typical traits of cellular senescence. Strikingly, both CAFs and HPFs stimulated with TGF-β are β-Gal and γ-H2AX-positive, thus suggesting a strict correlation between senescent cells and activated fibroblasts (Figure 5A,B). To corroborate this hypothesis, we investigated whether senescence-related gene signatures could correlate with activated fibroblasts. Gene Set Enrichment Analysis (GSEA) demonstrated an enrichment of a gene set up-regulated in senescent fibroblasts upon p53 inactivation (TANG_SENESCENCE_TP53_TARGETS_UP) among genes that are down-regulated during fibroblast activation, either occurring *in vivo* by contact with tumor cells (i.e. CAFs) or *in vitro* by stimulation with TGF-β (Supplementary Table 1). On the other hand, genes that are down-modulated upon p53 inactivation, hence likely favoring the establishment of senescence (TANG_SENESCENCE_TP53_TARGETS_DN), were found to be enriched in genes up-regulated in patient-derived CAFs (Supplementary Table 1). These correlations suggest a potential common transcriptional program between CAFs and senescent cells.

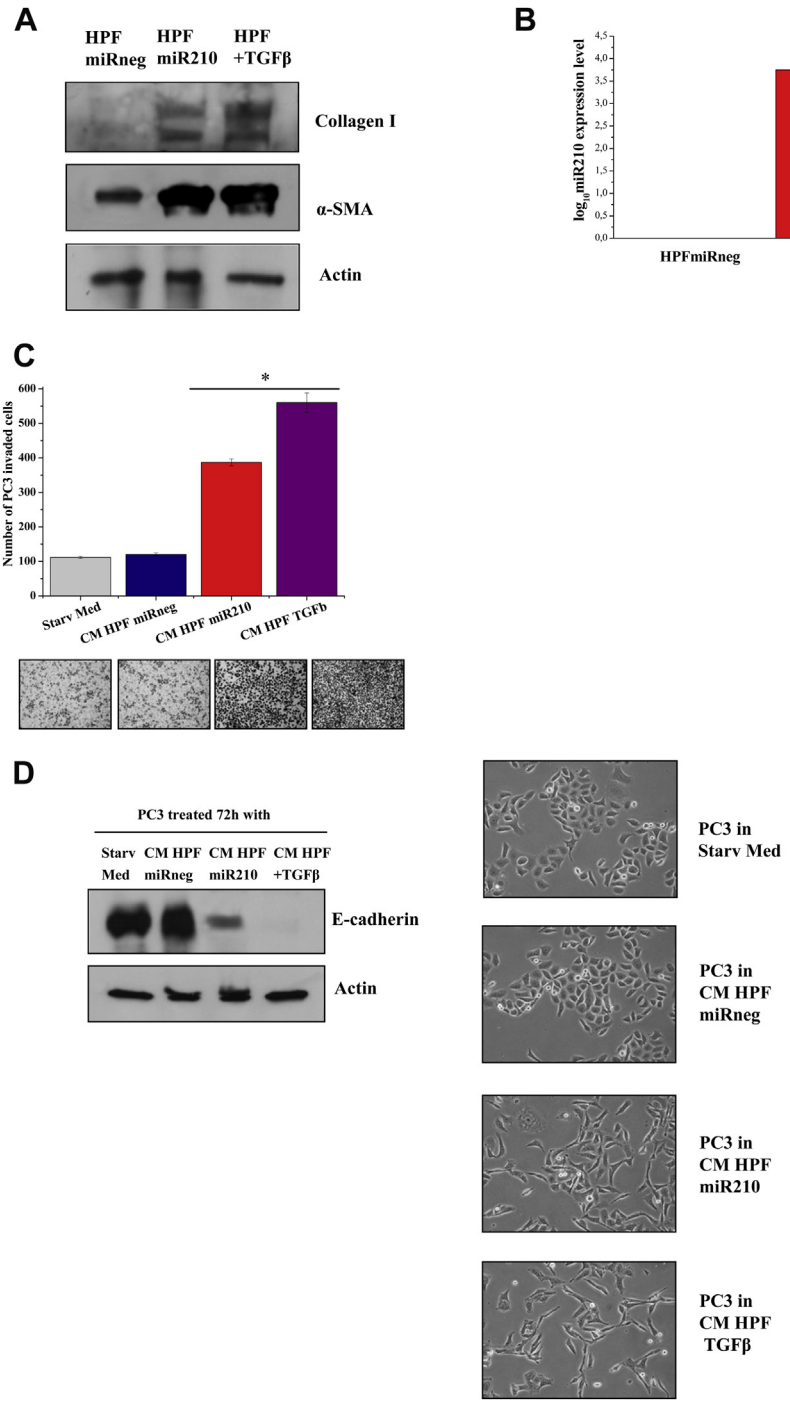

Figure 6 – *miR-210* induces fibroblasts activation and promotes PCa invasiveness. A) HPFs were transfected with *miR-210* or miRneg for 48 h. HPFs treated with 10 ng/ml TGF-β for 48 h were used as control of fibroblasts activation. Collagen I and α–SMA expression was assessed by immunoblot analysis. B) qRT-PCR measurement of *miR-210* expression levels in HPFs after 48 h of transfection with *miR-210* or miRneg. *$p < 0.005$ *miR-210* transfected cells *vs* miRneg transfected cells. C) PC3 cells were incubated for 48 h with CM derived from HPFs treated as in A, PC3 cells were then allowed to invade for 24 h through the filter coated with Matrigel toward the lower compartment filled with complete growth medium. Photographs are representative of four randomly chosen fields. *$p < 0.005$ CM *miR-210* transfected cells or TGF-β *vs* CM miRneg transfected cells. D) E-cadherin expression was assessed by immunoblot analysis on cell lysates of PC3 treated for 72 h with CM derived by HPFs treated as in A). Photographs of representative fields are shown.

miRNAs are key regulators of gene expression. Changes in the expression/regulation of a single miRNA could influence several genes and hence several cellular functions. *miR-210* is a hypoxia-associated miRNA. In line with what has been described in several models, human prostatic fibroblasts show a six-fold increase of *miR-210* expression levels when cultured in hypoxic condition (Supplemenatry Figure 2). Furthermore, Faraonio and colleagues have recently reported

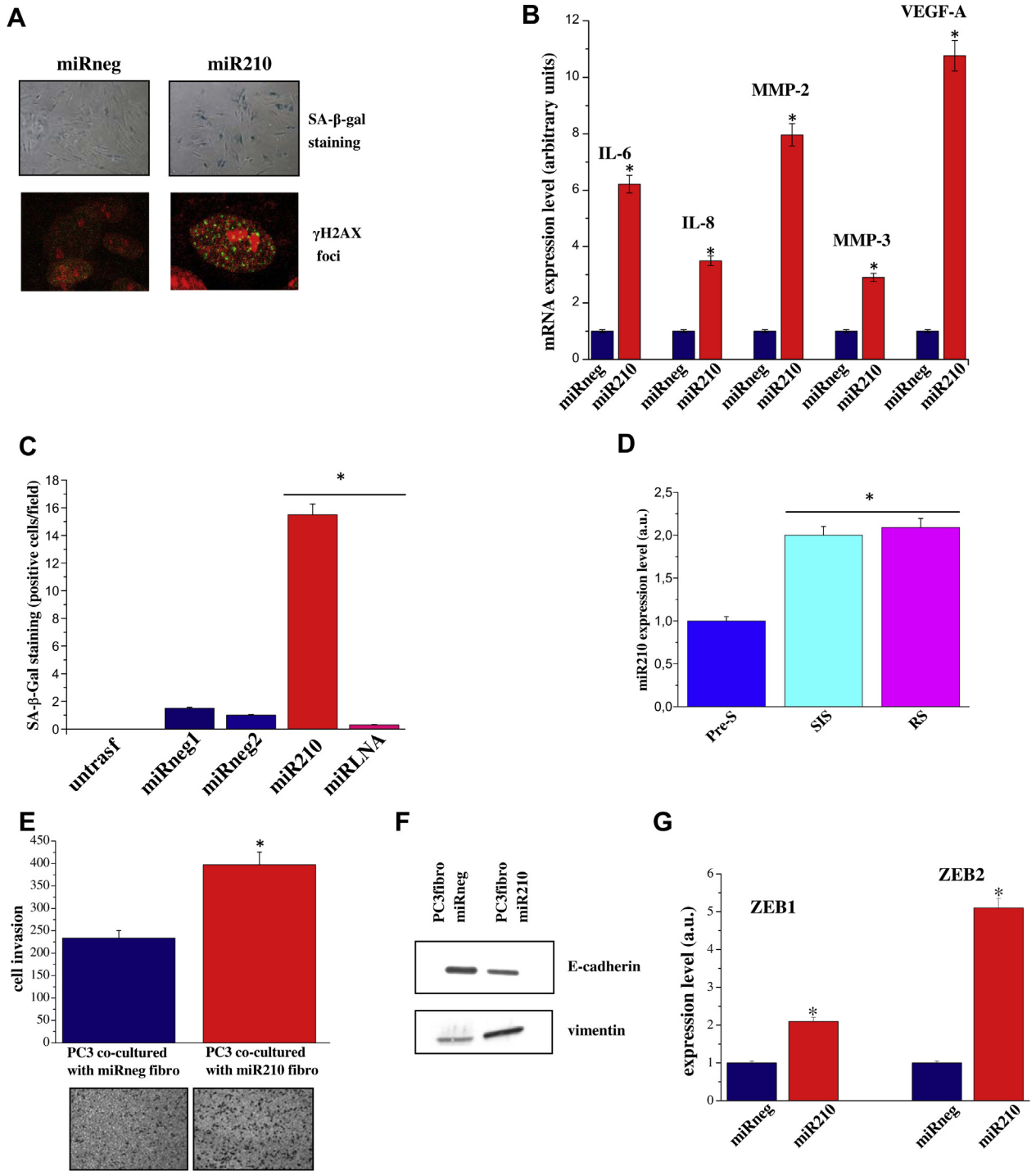

Figure 7 – *miR-210* overexpression induces cellular senescence: stimulation of PCa invasiveness, metabolic reprogramming an *in vitro* angiogenesis. A) HPFs were transfected with *miR-210* or miRneg. After 1 week cells were stained for SA-β-Gal, or fixed and examined by immunofluorescence for H2AX phosphorylated on Ser139 (γ-H2AX) and counterstained with propidium iodide. B) Total RNA was extracted from cells treated as in A) and IL-6, IL-8, MMP-2 MMP-3, and VEGF-A mRNA expression level were analyzed by qRT-PCR. Results are representative of three experiments with similar results. *$p < 0.005$ *miR-210* transfected HPFs *vs* miRneg transfected fibroblasts C) HPFs were transfected with *miR-210*, miRneg1, miRneg2. After 48 h miR-LNA inhibitor was ectopically overexpressed in *miR-210* transfected HPF. After 1 week cells were stained for SA-β-Gal. The bar graphs represent the mean of SA-β-Gal positive cells in six randomly chosen fields of triplicate experiments. *$p < 0.005$ *miR-210* and miR-LNA inhibitor transfected HPFs *vs* miRneg transfected HPFs. D) qRT-PCR measurement of *miR-210* expression levels in pre-senescent or senescent fibroblasts. *$p < 0.005$ senescent cells *vs* pre-senescent cells. E) HPFs were transfected with *miR-210* or miRneg. After 72 h PC3 cells were added to fibroblasts and co-cultured for further 72 h. Cells were then separated and 8×10^4 PC3 cells were subjected to invasion assay using a Boyden chamber. Invading cells were counted, and a bar graph, representative of six randomly chosen fields, is shown. *$p < 0.005$ PC3 cells transfected with *miR-210* cells *vs* PC3 cells transfected with miRneg. Cells treated as described, and (F) total

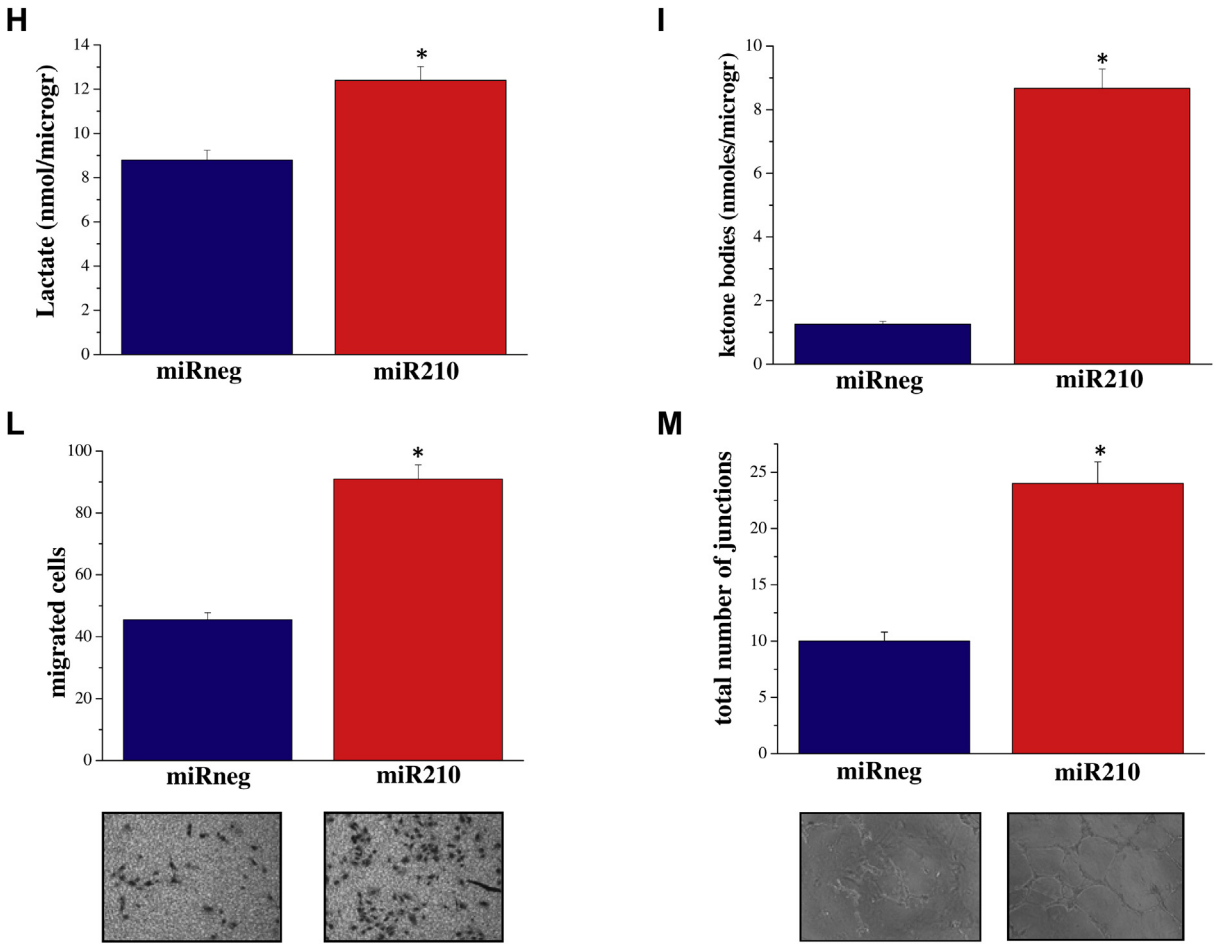

Figure 7 — *(continued)*

the up regulation of *miR-210* during cell senescence (Faraonio et al., 2012). Importantly, transfection of fibroblasts with the *miR-210* synthetic precursor caused a marked increase in α-SMA and collagen type I expression (Figure 6A,B), established features of fibroblasts activation. Consequently, *miR-210* seems to be the potential candidate to link hypoxia, fibroblasts senescence and activation in our experimental model. Accordingly, CM from *miR-210* transfected fibroblasts induced increased invasiveness and a clear EMT in PC3 cancer cells (Figure 6C,D). To support the link between fibroblasts activation and SASP, we demonstrated that CM from *miR-210* ectopically expressing fibroblasts, treated with IL6/IL8 blocking antibodies or Ilomastat, impairs PC3 invasiveness (Supplementary Figure 3). We demonstrated that *miR-210* overexpression has a key role in the induction of cell senescence when transfected in pre-senescent cells as shown by positive staining with SA-β-Gal and γ-H2AX foci (Figure 7A). In keeping with a central role of *miR-210* in the induction of cell senescence, *miR-210* ectopically expression activates the SASP, as shown by increased levels of IL-6, IL-8, VEGF-A, MMP3, MMP2 transcripts (Figure 7B). In agreement, LNA-mediated *miR-210* silencing was able to revert senescence induction as demonstrated by the marked decrease in the number of SA-β-Gal-positive cells (Figure 7C). We next investigated whether *miR-210* levels were up-regulated in fibroblasts undergoing RS and SIS. As demonstrated by quantitative Real

cell lysates were subject to immunoblot to evaluate E-cadherin and vimentin or (G) used for total RNA extraction and quantification of ZEB1 and ZEB2 mRNA expression level by qRT-PCR. The results are representative of three experiments with similar results. *$p < 0.005$ *miR-210* transfected HPFs *vs* miRneg transfected HPFs. H–I) HPFs were transfected with *miR-210* or miRneg. After 72 h cells were serum starved for 24 h and then Lactate assay and ketone bodies assay were performed. *$p < 0.005$ *miR-210* transfected HPFs *vs* miRneg transfected HPFs. L) EPC cells, after 24 h of serum starvation, were seeded into the upper compartment of Boyden chamber. Cells were allowed to migrate through the filter toward the lower compartment filled with CM of HPFs transfected with *miR-210* or miRneg. *$p < 0.005$ *miR-210* transfected HPFs *vs* miRneg transfected fibroblasts. M) HUVECs were seeded on Matrigel coated plate in presence of CM of HPFs transfected with *miR-210* or miRneg. Cord formation was examined by phase-contrast microscopy. The total number of junctions for optical field is counted. Results are representative of three independent experiments. *$p < 0.005$ *miR-210* transfected HPFs *vs* miRneg transfected fibroblasts.

Time RT-PCR, *miR-210* expression levels increased in both cell models, confirming the link between *miR-210* expression and cell senescence (Figure 7D). Furthermore, co-culturing PC3 cells with *miR-210* transfected fibroblasts induced an increase in cancer cell invasiveness (Figure 7E). Cancer cells invasiveness was associated with EMT traits as shown by decreased expression of E-cadherin and increased expression of vimentin, ZEB1 and ZEB2 (Figure 7F,G). Senescent fibroblasts induced by *miR-210* expression can produce energy-rich metabolites, such as L-lactate and ketone bodies to fuel tumor cell growth, similar to what has been demonstrated for activated fibroblasts (Figure 7H,I). In keeping with the already observed key role of senescent fibroblasts in the activation of microenvironmental components, we found that *miR-210* expressing senescent fibroblasts affect the recruitment of EPCs and HUVEC capillary morphogenesis (Figure 7L,M), thus confirming a central role of senescent stroma in promoting cancer growth and dissemination.

Finally, to emphasize the importance of senescence in tumor progression, we analyzed whether the typical markers of senescence have a role in prostate cancer progression. Data mining of publicly available tumor datasets highlights the importance of senescent related marker in prostate cancer progression. By analyzing a cohort of 171 samples (GSE6919), *miR-210* expression levels is significantly higher in metastatic prostate cancers when compared to normal tissue, tissue adjacent to tumor site and primary prostate cancers, all displaying similar expression levels (Figure 8A). In the same dataset, both *MMP3* (Figure 8B) and *IL-8* (Figure 8C) expression levels are enhanced in metastatic prostate cancers when compared to primary tumors. Importantly, both primary tumor and tissue adjacent to tumor show a higher expression of *IL-8* when compared to normal prostate tissue. This could be explained by the higher inflammatory response that characterizes the tumor sites when compared to normal prostate tissue. Serum IL-6 levels have a prognostic relevance in prostate cancer (Nakashima et al., 2000) and IL-6 can promote prostate tumorigenesis (Rojas et al., 2011). By analyzing a cohort of 179 samples (GSE21032), we found that *IL-6* expression is significantly increased in the tumor samples when compared to normal prostate tissue (Figure 8D). Finally, the analysis of a small cohort of prostate cancer patients showed a higher *MMP2* expression levels in the tumor samples, with a borderline statistical significance (Figure 8E).

4. Discussion

Data herein presented show the central role of hypoxic senescent stroma in stimulating prostate tumor cell aggressiveness, acting not only on cancer cells themselves, but also sustaining a reactive microenvironment able to positively influence inflammation and angiogenesis. Moreover, we pointed out a fascinating role for *miR-210* in mediating, at least in part, these phenomena. The hypoxia-associated miRNA, *miR-210* has been previously identified as upregulated during both replicative and chemically induced senescence of human diploid fibroblasts (Faraonio et al., 2012). Oxidative stress and DNA damage, which promote replicative senescence, induce *miR-210* expression that favors DNA damage and oxidative stress creating a vicious loop to sustain cell senescence (Faraonio et al., 2012). Little is known about the molecular targets of *miR-210* involved in cell senescence. However, *miR210* induction has been reported to associated with the down regulation of iron–sulfur cluster scaffold protein homolog and cytochrome-c oxidase assembly protein responsible for the decrease of mitochondrial function and the increase of reactive oxygen species (ROS) (Chen et al., 2010). In addition, the overexpression of *miR-210* affects the expression levels of several subunits of the electron transport chain complexes I and II, including the subunit D of succinate dehydrogenase complex, thus leading to mitochondrial dysfunction in lung adenocarcinoma A549 cells (Puissegur et al., 2011). In keeping with the close link between cell senescence and DNA damage, forced expression of *miR-210* was found to suppress the levels of RAD52, which is a key factor in DNA repair by homologous recombination (Crosby et al., 2009). In addition, *miR-210* is able to affect also cell cycle progression, by targeting E2F transcription factor 3 and the fibroblast growth factor receptor like 1 (Biswas et al., 2010; Tsuchiya et al., 2011). Furthermore, Overhoff et al. demonstrated that *miR-210* enhanced expression leads to the repression of members of Polycomb group proteins, thereby activating p16 to promote senescence (Overhoff et al., 2014).

Our data identify *miR-210* as a "trait d'union" molecule between hypoxia-induced cell senescence and fibroblast activation. In fact, the ectopic overexpression of *miR-210* converted healthy fibroblasts into CAFs as assessed by α-SMA and collagen type I increased expression levels (Figure 6A). Indeed, the senescence-inducing stimuli used in our work (e.g. H_2O_2 treatment and oxidative stress) have been also described to induce myofibroblasts differentiation and to promote autophagy in CAFs (Liu et al., 2011; Tian et al., 2011; Waghray et al., 2005). In fact, mesenchymal–mesenchymal transition is strongly dependent on oxidative stress in both neoplastic and fibrotic disease (Amara et al., 2010; Bocchino et al., 2010; Giannoni et al., 2012). In a model of tumor–stroma interaction of skin carcinogenesis, Cat et al. reported that TGF-β-induced transdifferentiation of fibroblasts is a ROS-dependent event (Cat et al., 2006). Moreover, Toullec et al. showed that ROS can promote the conversion of fibroblasts into highly migrating myofibroblasts in a HIF-1 dependent mechanism (Toullec et al., 2010). Thus, oxidative stress is the driving force for both activation and establishment of the senescent phenotype of fibroblasts. Senescent and activated fibroblasts have similar phenotypes. In fact, the activated fibroblasts have increased levels of *miR-210*, acquire a secretory phenotype, increase their proliferation and can establish a cross-talk with the surrounding tissues by sustaining EMT of cancer cells and activating monocytes and endothelial cells (Comito et al., 2014; Fiaschi et al., 2012; Giannoni et al., 2011). Moreover, we have previously reported, along with others, that CAFs can promote tumor progression by sustaining inflammation (Giannoni et al., 2011; Kalluri and Zeisberg, 2006). CAFs mediate the inflammatory response by secreting chemokines such as monocyte chemotactic

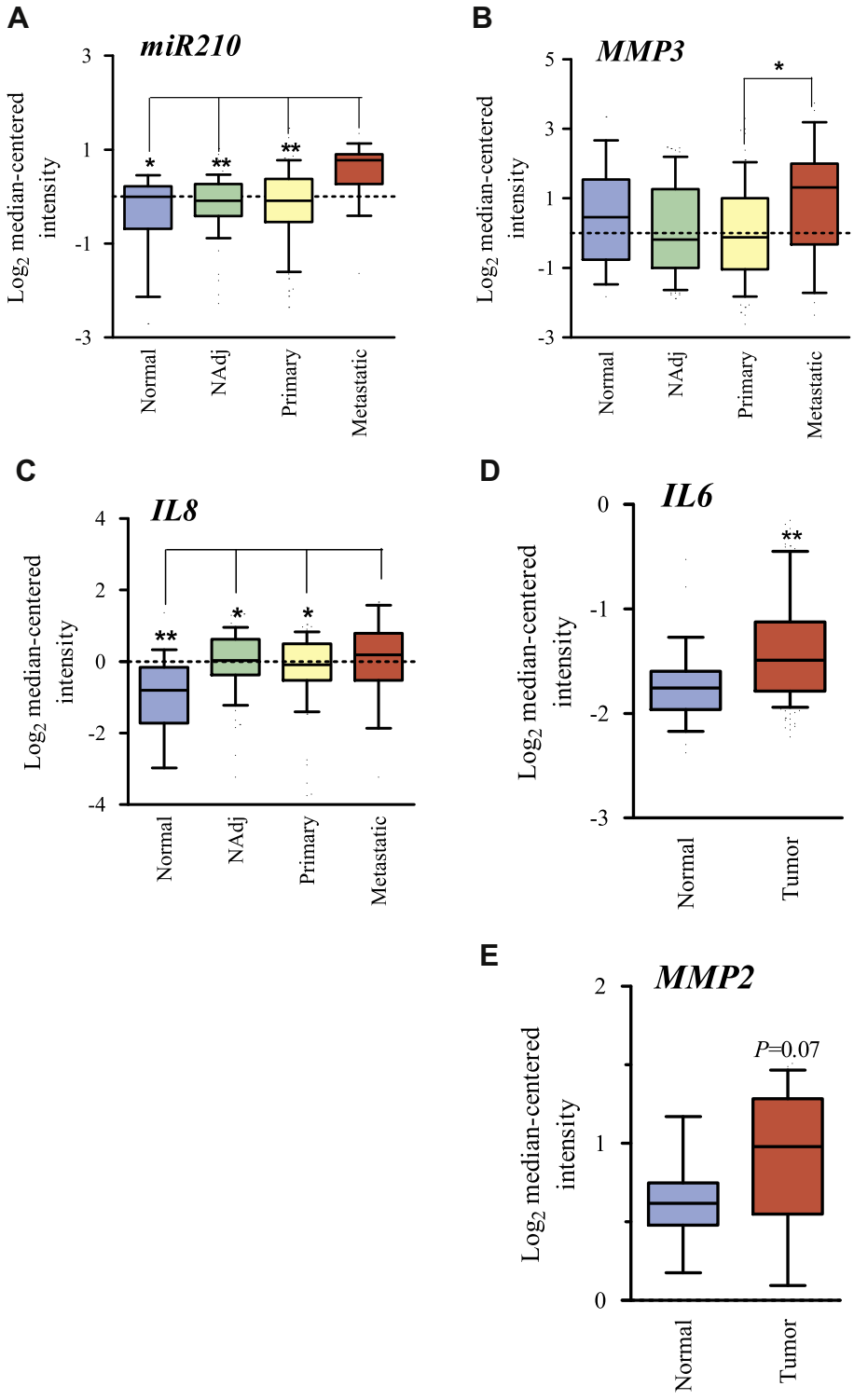

Figure 8 – Gene expression analysis of senescence-related genes in publicly available prostate cancer datasets. (A–C) *miR-210HG* (44211_at), *MMP3* (437_at) and *IL8* (35372_r_at) transcripts expression levels are shown for normal prostate tissues ($n = 18$), normal prostate tissues adjacent to tumor (NAdj, $n = 63$) primary ($n = 65$) and metastatic ($n = 25$) prostate cancers (GSE6919). One-way ANOVA and Dunnett posthoc test were used for the analysis. D) *IL6* (ID564) gene expression levels is shown for normal prostate tissues ($n = 29$) and prostate cancers ($n = 150$) (GSE21032). Student *t*-test was used for the analysis. $^{*}p < 0.05$, $^{**}p < 0.01$. E) *MMP2* (39007_at) gene expression levels is shown for normal prostate tissues ($n = 9$) and prostate cancers ($n = 25$) in Welsh dataset. Student *t*-test was used for the analysis.

protein 1, stromal cell-derived factor 1 (SDF-1) and inflammatory factors like IL-1, IL-6, COX-2 and chemokine (C-X-C motif) ligand 1 (Erez et al., 2010, 2013; Kalluri and Zeisberg, 2006). Indeed, SDF-1 secretion is responsible for CAF-mediated monocytes recruitment (Comito et al., 2014). Furthermore, CAFs positively affect the development of a capillary network able to oxygenate tumor. In breast and prostate carcinomas, CAFs have been involved in recruiting EPCs, through the secretion of SDF-1, thereby promoting tumor vascularization (Giannoni et al., 2013; Orimo et al., 2005). In this work, we demonstrate that SIS, RS as well as senescence induced by *miR-210* overexpression lead to the recruitment of both monocytes and endothelial cells to support tumor growth. In keeping, we demonstrated that CAFs, isolated from aggressive human tumors are strongly positive for β-Gal and γ-H2AX foci and share a common transcriptional program with senescent fibroblasts (Figure 5 and Suppl. Table 1). These results are in agreement with previous published data showing that fibroblast stimulation with TGF-β1 induces a senescent-like morphology, SA-β-Gal activity and overexpression of senescence-associated genes (Frippiat et al., 2001). Conversely, Untergasser's group reveals several variations between cell senescence and TGF-β induced fibroblast activation, such as the absence of α-SMA expression in senescent cells or the lack of β-Gal positivity in TGF-β stimulated fibroblasts. Nevertheless, both senescent cells and TGF-β-activated fibroblasts showed increased secretion of growth factors, cytokines and components of the extracellular matrix and degrading enzymes, as well as the ability to support tumor growth (Bavik et al., 2006; Laberge et al., 2012; Untergasser et al., 2005). Indeed, the two models are not completely overlapping, as evidenced by the fact that senescent cells completely lose their proliferation ability while TGF-β-activated fibroblasts are only reversibly growth inhibited. However, senescence and fibroblast activation certainly share many common features that make these two cell types similarly active in promoting tumor growth. In keeping with this idea, hypoxia synergizes with both tumor progression due to CAFs contact (Comito et al., 2012) and with senescence of fibroblasts (Coppe et al., 2008). Moreover, CAFs used in our study were isolated from tumor samples and not TGF-β activated *in vitro*. The different sources of CAF strongly validated our initial hypothesis.

In keeping with the trophic effect exerted by senescent fibroblasts (see Figures 2 and 7) the group of Lisanti demonstrated that autophagic CAFs produce high-energy metabolites to fuel cancer growth, induce p21 expression and a morphologic cell hypertrophy associated with the induction of β-Gal activity suggesting that senescent fibroblasts and autophagic CAFs are two sides of the same coin (Capparelli et al., 2012). In addition, senescent fibroblasts shift their metabolism toward aerobic glycolysis as demonstrated for CAFs (Goldstein et al., 1982; Stockl et al., 2006). Interestingly, Capparelli et al. show that the distribution of β-Gal in human breast cancers is largely confined to the tumor stroma, reflecting the onset of senescence in the tumor microenvironment (Capparelli et al., 2012). Similar results were obtained also by Yang et al., in human ovarian cancer where stromal fibroblasts adjacent to epithelial cancer cells (and possibly tumor-educated/activated), are senescent (Yang et al., 2006).

5. Conclusions

In summary, we have demonstrated that hypoxia-induced senescent stroma is a key feature of PCa malignancy. Particularly, our data highlight a great degree of similarity between stroma activation (induced by cancer cell) and senescence. Notably, the hypoxia-mediated *miR-210* has a central role both in cell senescence induction and in mediating several CAF features, as the recruitment of inflammatory cells, tumor vessels formation and in the production of high-energy metabolites to sustain cancer growth. Consequently, systemic therapeutic approaches that impair *miR-210* function/expression could decrease the senescent-associated phenotype of cancer-associated stromal cells and therefore reduce the cancer aggressiveness. These data highlight the importance of developing *miR-210*-based approaches to prevent and treat prostate metastatic disease.

Conflict-of-interest disclosure

The authors declare no competing interests.

Regione Toscana
POR Creo 2007-13 PROGRAMMA OPERATIVO REGIONALE OBIETTIVO COMPETITIVITÀ REGIONALE e OCCUPAZIONE Fondo Europeo di Sviluppo Regionale
REPUBBLICA ITALIANA
Unione Europea
Le ali alle tue idee

Acknowledgments

The work was supported by Associazione Italiana Ricerca sul Cancro (AIRC), grants # 11542 (P.G.), grants # 8797 (P.C.), Istituto Toscano Tumori (grants # 0203607) (P.C.), by a fellowship from Fondazione Italiana Ricerca sul Cancro (FIRC) to A.M, Special Program "Innovative Tools for Cancer Risk Assessment and Early Diagnosis", 5X1000, (grant # 12162), (N.Z.) and by Programma operativo regionale Obiettivo "Competitività regionale e occupazione" della Regione Toscana cofinanziato dal Fondo europeo di sviluppo regionale 2007–2013 (POR CReO FESR 2007–2013) and Fondazione Italo Monzino (N.Z.).

Appendix A. Supplementary data

Supplementary data related to this article can be found at http://dx.doi.org/10.1016/j.molonc.2014.07.009.

REFERENCES

Aisner, D.L., Wright, W.E., Shay, J.W., 2002. Telomerase regulation: not just flipping the switch. Curr. Opin. Genet. Dev. 12, 80–85.

Amara, N., Goven, D., Prost, F., Muloway, R., Crestani, B., Boczkowski, J., 2010. NOX4/NADPH oxidase expression is increased in pulmonary fibroblasts from patients with idiopathic pulmonary fibrosis and mediates TGFbeta1-induced fibroblast differentiation into myofibroblasts. Thorax 65, 733–738.

Bavik, C., Coleman, I., Dean, J.P., Knudsen, B., Plymate, S., Nelson, P.S., 2006. The gene expression program of prostate fibroblast senescence modulates neoplastic epithelial cell proliferation through paracrine mechanisms. Cancer Res. 66, 794–802.

Biswas, S., Roy, S., Banerjee, J., Hussain, S.R., Khanna, S., Meenakshisundaram, G., Kuppusamy, P., Friedman, A., Sen, C.K., 2010. Hypoxia inducible microRNA 210 attenuates keratinocyte proliferation and impairs closure in a murine model of ischemic wounds. Proc. Natl. Acad. Sci. U. S. A. 107, 6976–6981.

Bocchino, M., Agnese, S., Fagone, E., Svegliati, S., Grieco, D., Vancheri, C., Gabrielli, A., Sanduzzi, A., Avvedimento, E.V., 2010. Reactive oxygen species are required for maintenance and differentiation of primary lung fibroblasts in idiopathic pulmonary fibrosis. PLoS One 5, e14003.

Campisi, J., Andersen, J.K., Kapahi, P., Melov, S., 2011. Cellular senescence: a link between cancer and age-related degenerative disease? Semin. Cancer Biol. 21, 354–359.

Capparelli, C., Guido, C., Whitaker-Menezes, D., Bonuccelli, G., Balliet, R., Pestell, T.G., Goldberg, A.F., Pestell, R.G., Howell, A., Sneddon, S., Birbe, R., Tsirigos, A., Martinez-Outschoorn, U., Sotgia, F., Lisanti, M.P., 2012. Autophagy and senescence in cancer-associated fibroblasts metabolically supports tumor growth and metastasis via glycolysis and ketone production. Cell Cycle 11, 2285–2302.

Cat, B., Stuhlmann, D., Steinbrenner, H., Alili, L., Holtkotter, O., Sies, H., Brenneisen, P., 2006. Enhancement of tumor invasion depends on transdifferentiation of skin fibroblasts mediated by reactive oxygen species. J.Cell Sci. 119, 2727–2738.

Chen, Q., Fischer, A., Reagan, J.D., Yan, L.J., Ames, B.N., 1995. Oxidative DNA damage and senescence of human diploid fibroblast cells. Proc. Natl. Acad. Sci. U. S. A. 92, 4337–4341.

Chen, Z., Li, Y., Zhang, H., Huang, P., Luthra, R., 2010. Hypoxia-regulated microRNA-210 modulates mitochondrial function and decreases ISCU and COX10 expression. Oncogene 29, 4362–4368.

Cirri, P., Chiarugi, P., 2012. Cancer-associated-fibroblasts and tumour cells: a diabolic liaison driving cancer progression. Cancer Metastasis Rev. 31, 195–208.

Comito, G., Giannoni, E., Segura, C.P., Barcellos-de-Souza, P., Raspollini, M.R., Baroni, G., Lanciotti, M., Serni, S., Chiarugi, P., 2014. Cancer-associated fibroblasts and M2-polarized macrophages synergize during prostate carcinoma progression. Oncogene 33, 2423–2431.

Comito, G., Giannoni, E., Di Gennaro, P., Segura, C.P., Gerlini, G., Chiarugi, P., 2012. Stromal fibroblasts synergize with hypoxic oxidative stress to enhance melanoma aggressiveness. Cancer Lett. 324, 31–41.

Coppe, J.P., Desprez, P.Y., Krtolica, A., Campisi, J., 2010. The senescence-associated secretory phenotype: the dark side of tumor suppression. Annu. Rev. Pathol. 5, 99–118.

Coppe, J.P., Patil, C.K., Rodier, F., Sun, Y., Munoz, D.P., Goldstein, J., Nelson, P.S., Desprez, P.Y., Campisi, J., 2008. Senescence-associated secretory phenotypes reveal cell-nonautonomous functions of oncogenic RAS and the p53 tumor suppressor. PLoS Biol. 6, 2853–2868.

Crosby, M.E., Kulshreshtha, R., Ivan, M., Glazer, P.M., 2009. MicroRNA regulation of DNA repair gene expression in hypoxic stress. Cancer Res. 69, 1221–1229.

DePinho, R.A., 2000. The age of cancer. Nature 408, 248–254.

Di, L.A., Linke, S.P., Clarkin, K., Wahl, G.M., 1994. DNA damage triggers a prolonged p53-dependent G1 arrest and long-term induction of Cip1 in normal human fibroblasts. Genes Dev. 8, 2540–2551.

Dolle, M.E., Snyder, W.K., Dunson, D.B., Vijg, J., 2002. Mutational fingerprints of aging. Nucleic Acids Res. 30, 545–549.

Erez, N., Glanz, S., Raz, Y., Avivi, C., Barshack, I., 2013. Cancer associated fibroblasts express pro-inflammatory factors in human breast and ovarian tumors. Biochem. Biophys. Res. Commun. 437, 397–402.

Erez, N., Truitt, M., Olson, P., Arron, S.T., Hanahan, D., 2010. Cancer-associated fibroblasts are activated in incipient neoplasia to orchestrate tumor-promoting inflammation in an NF-kappaB-dependent manner. Cancer Cell 17, 135–147.

Faraonio, R., Salerno, P., Passaro, F., Sedia, C., Iaccio, A., Bellelli, R., Nappi, T.C., Comegna, M., Romano, S., Salvatore, G., Santoro, M., Cimino, F., 2012. A set of miRNAs participates in the cellular senescence program in human diploid fibroblasts. Cell Death Differ. 19, 713–721.

Fiaschi, T., Marini, A., Giannoni, E., Taddei, M.L., Gandellini, P., De, D.A., Lanciotti, M., Serni, S., Cirri, P., Chiarugi, P., 2012. Reciprocal metabolic reprogramming through lactate shuttle coordinately influences tumor-stroma interplay. Cancer Res. 72, 5130–5140.

Frippiat, C., Chen, Q.M., Zdanov, S., Magalhaes, J.P., Remacle, J., Toussaint, O., 2001. Subcytotoxic H2O2 stress triggers a release of transforming growth factor-beta 1, which induces biomarkers of cellular senescence of human diploid fibroblasts. J. Biol. Chem. 276, 2531–2537.

Giannoni, E., Bianchini, F., Calorini, L., Chiarugi, P., 2011. Cancer associated fibroblasts exploit reactive oxygen species through a proinflammatory signature leading to epithelial mesenchymal transition and stemness. Antioxid. Redox Signal 14, 2361–2371.

Giannoni, E., Bianchini, F., Masieri, L., Serni, S., Torre, E., Calorini, L., Chiarugi, P., 2010. Reciprocal activation of prostate cancer cells and cancer-associated fibroblasts stimulates

epithelial-mesenchymal transition and cancer stemness. Cancer Res. 70, 6945–6956.
Giannoni, E., Parri, M., Chiarugi, P., 2012. EMT and oxidative stress: a bidirectional interplay affecting tumor malignancy. Antioxid. Redox Signal 16, 1248–1263.
Giannoni, E., Taddei, M.L., Parri, M., Bianchini, F., Santosuosso, M., Grifantini, R., Fibbi, G., Mazzanti, B., Calorini, L., Chiarugi, P., 2013. EphA2-mediated mesenchymal-amoeboid transition induced by endothelial progenitor cells enhances metastatic spread due to cancer-associated fibroblasts. J. Mol. Med. (Berl.) 91, 103–115.
Goldstein, S., Ballantyne, S.R., Robson, A.L., Moerman, E.J., 1982. Energy metabolism in cultured human fibroblasts during aging in vitro. J. Cell. Physiol. 112, 419–424.
Hanahan, D., Weinberg, R.A., 2011. Hallmarks of cancer: the next generation. Cell 144, 646–674.
Harris, A.L., 2002. Hypoxia – a key regulatory factor in tumour growth. Nat. Rev. Cancer 2, 38–47.
Hayflick, L., 1965. The limited in vitro lifetime of human diploid cell strains. Exp. Cell Res. 37, 614–636.
Kalluri, R., Zeisberg, M., 2006. Fibroblasts in cancer. Nat. Rev. Cancer 6, 392–401.
Kim Sh, S.H., Kaminker, P., Campisi, J., 2002. Telomeres, aging and cancer: in search of a happy ending. Oncogene 21, 503–511.
Kimura, M., Stone, R.C., Hunt, S.C., Skurnick, J., Lu, X., Cao, X., Harley, C.B., Aviv, A., 2010. Measurement of telomere length by the Southern blot analysis of terminal restriction fragment lengths. Nat. Protoc. 5, 1596–1607.
Krtolica, A., Campisi, J., 2002. Cancer and aging: a model for the cancer promoting effects of the aging stroma. Int. J. Biochem. Cell Biol. 34, 1401–1414.
Krtolica, A., Parrinello, S., Lockett, S., Desprez, P.Y., Campisi, J., 2001. Senescent fibroblasts promote epithelial cell growth and tumorigenesis: a link between cancer and aging. Proc. Natl. Acad. Sci. U. S. A. 98, 12072–12077.
Laberge, R.M., Awad, P., Campisi, J., Desprez, P.Y., 2012. Epithelial-mesenchymal transition induced by senescent fibroblasts. Cancer Microenviron. 5, 39–44.
Liu, D.H., Chen, Y.M., Liu, Y., Hao, B.S., Zhou, B., Wu, L., Wang, M., Chen, L., Wu, W.K., Qian, X.X., 2011. Rb1 protects endothelial cells from hydrogen peroxide-induced cell senescence by modulating redox status. Biol. Pharm. Bull. 34, 1072–1077.
Margheri, F., Chilla, A., Laurenzana, A., Serrati, S., Mazzanti, B., Saccardi, R., Santosuosso, M., Danza, G., Sturli, N., Rosati, F., Magnelli, L., Papucci, L., Calorini, L., Bianchini, F., Del, R.M., Fibbi, G., 2011. Endothelial progenitor cell-dependent angiogenesis requires localization of the full-length form of uPAR in caveolae. Blood 118, 3743–3755.
Nakashima, J., Tachibana, M., Horiguchi, Y., Oya, M., Ohigashi, T., Asakura, H., Murai, M., 2000. Serum interleukin 6 as a prognostic factor in patients with prostate cancer. Clin. Cancer Res. 7, 2702–2706.
Ogryzko, V.V., Hirai, T.H., Russanova, V.R., Barbie, D.A., Howard, B.H., 1996. Human fibroblast commitment to a senescence-like state in response to histone deacetylase inhibitors is cell cycle dependent. Mol. Cell Biol. 16, 5210–5218.
Orimo, A., Gupta, P.B., Sgroi, D.C., Arenzana-Seisdedos, F., Delaunay, T., Naeem, R., Carey, V.J., Richardson, A.L., Weinberg, R.A., 2005. Stromal fibroblasts present in invasive human breast carcinomas promote tumor growth and angiogenesis through elevated SDF-1/CXCL12 secretion. Cell 121, 335–348.
Overhoff, M.G., Garbe, J.C., Koh, J., Stampfer, M.R., Beach, D.H., Bishop, C.L., 2014. Cellular senescence mediated by p16INK4A-coupled miRNA pathways. Nucleic Acids Res 42, 1606–1618.
Parrinello, S., Coppe, J.P., Krtolica, A., Campisi, J., 2005. Stromal-epithelial interactions in aging and cancer: senescent fibroblasts alter epithelial cell differentiation. J. Cell Sci. 118, 485–496.
Pietras, K., Ostman, A., 2010. Hallmarks of cancer: interactions with the tumor stroma. Exp. Cell Res. 316, 1324–1331.
Puissegur, M.P., Mazure, N.M., Bertero, T., Pradelli, L., Grosso, S., Robbe-Sermesant, K., Maurin, T., Lebrigand, K., Cardinaud, B., Hofman, V., Fourre, S., Magnone, V., Ricci, J.E., Pouyssegur, J., Gounon, P., Hofman, P., Barbry, P., Mari, B., 2011. miR-210 is overexpressed in late stages of lung cancer and mediates mitochondrial alterations associated with modulation of HIF-1 activity. Cell Death Differ. 18, 465–478.
Robles, S.J., Adami, G.R., 1998. Agents that cause DNA double strand breaks lead to p16INK4a enrichment and the premature senescence of normal fibroblasts. Oncogene 16, 1113–1123.
Rojas, A., Liu, G., Coleman, I., Nelson, P.S., Zhang, M., Dash, R., Fisher, P.B., Plymate, S.R., Wu, J.D., 2011. IL-6 promotes prostate tumorigenesis and progression through autocrine cross-activation of IGF-IR. Oncogene 30, 2345–2355.
Serrano, M., Lin, A.W., McCurrach, M.E., Beach, D., Lowe, S.W., 1997. Oncogenic ras provokes premature cell senescence associated with accumulation of p53 and p16INK4a. Cell 88, 593–602.
Stockl, P., Hutter, E., Zwerschke, W., Jansen-Durr, P., 2006. Sustained inhibition of oxidative phosphorylation impairs cell proliferation and induces premature senescence in human fibroblasts. Exp. Gerontol. 41, 674–682.
Tchkonia, T., Zhu, Y., van, D.J., Campisi, J., Kirkland, J.L., 2013. Cellular senescence and the senescent secretory phenotype: therapeutic opportunities. J. Clin. Invest. 123, 966–972.
Tian, L.M., Xie, H.F., Xiao, X., Yang, T., Hu, Y.H., Wang, W.Z., Liu, L.S., Chen, X., Li, J., 2011. Study on the roles of beta-catenin in hydrogen peroxide-induced senescence in human skin fibroblasts. Exp. Dermatol. 20, 836–838.
Toullec, A., Gerald, D., Despouy, G., Bourachot, B., Cardon, M., Lefort, S., Richardson, M., Rigaill, G., Parrini, M.C., Lucchesi, C., Bellanger, D., Stern, M.H., Dubois, T., Sastre-Garau, X., Delattre, O., Vincent-Salomon, A., Mechta-Grigoriou, F., 2010. Oxidative stress promotes myofibroblast differentiation and tumour spreading. EMBO Mol. Med. 2, 211–230.
Tsuchiya, S., Fujiwara, T., Sato, F., Shimada, Y., Tanaka, E., Sakai, Y., Shimizu, K., Tsujimoto, G., 2011. MicroRNA-210 regulates cancer cell proliferation through targeting fibroblast growth factor receptor-like 1 (FGFRL1). J. Biol. Chem. 286, 420–428.
Untergasser, G., Gander, R., Lilg, C., Lepperdinger, G., Plas, E., Berger, P., 2005. Profiling molecular targets of TGF-beta1 in prostate fibroblast-to-myofibroblast transdifferentiation. Mech. Ageing Dev. 126, 59–69.
Waghray, M., Cui, Z., Horowitz, J.C., Subramanian, I.M., Martinez, F.J., Toews, G.B., Thannickal, V.J., 2005. Hydrogen peroxide is a diffusible paracrine signal for the induction of epithelial cell death by activated myofibroblasts. FASEB J. 19, 854–856.
Welsh, J.B., Sapinoso, L.M., Su, A.I., Kern, S.G., Wang-Rodriguez, J., Moskaluk, C.A., Frierson Jr., H.F., Hampton, G.M., 2001. Analysis of gene expression identifies candidate markers and pharmacological targets in prostate cancer. Cancer Res. 61, 5974–5978.
Yang, G., Rosen, D.G., Zhang, Z., Bast Jr., R.C., Mills, G.B., Colacino, J.A., Mercado-Uribe, I., Liu, J., 2006. The chemokine growth-regulated oncogene 1 (Gro-1) links RAS signaling to the senescence of stromal fibroblasts and ovarian tumorigenesis. Proc. Natl. Acad. Sci. U. S. A. 103, 16472–16477.